Journal of ELECTRONIC MATERIALS, Vol. 47, No. 8, 2018
https://doi.org/10.1007/s11664-018-6160-6

TOPICAL COLLECTION: ELECTRONIC MATERIALS FOR RENEWABLE ENERGY APPLICATIONS

Exploration of a Permanent Magnet Synchronous Generator with Compensated Reactance Windings in Parallel Rod Configuration

OLEG LYAN,[1] VALDAS JANKUNAS,[1] ELEONORA GUSEINOVIENE,[1,3] ALEKSAS PAŠILIS,[1] AUDRIUS SENULIS,[1] AUDRIUS KNOLIS,[1] and EROL KURT[2]

1.—Department of Engineering, Faculty of Marine Technology and Natural Sciences, Klaipeda University, Bijunu Str. 17, 91225 Klaipeda, Lithuania. 2.—Department of Electrical and Electronics Engineering, Technology Faculty, Gazi University, 06500 Besevler, Ankara, Turkey. 3.—e-mail: eleonora.guseinoviene@ku.lt

In this study, a permanent magnet synchronous generator (PMSG) topology with compensated reactance windings in parallel rod configuration is proposed to reduce the armature reactance X_L and to achieve higher efficiency of PMSG. The PMSG was designed using iron-cored bifilar coil topology to overcome problems of market-dominant rotary type generators. Often the problem is a comparatively high armature reactance X_L, which is usually bigger than armature resistance R_a. Therefore, the topology is proposed to partially compensate or negligibly reduce the PMSG reactance. The study was performed by using finite element method (FEM) analysis and experimental investigation. FEM analysis was used to investigate magnetic field flux distribution and density in PMSG. The PMSG experimental analyses of no-load losses and electromotive force versus frequency (i.e., speed) was performed. Also terminal voltage, power output and efficiency relation with load current at different frequencies have been evaluated. The reactance of PMSG has low value and a linear relation with operating frequency. The low reactance gives a small variation of efficiency (from 90% to 95%) in a wide range of load (from 3 A to 10 A) and operation frequency (from 44 Hz to 114 Hz). The comparison of PMSG characteristics with parallel and series winding connection showed insignificant power variation. The research results showed that compensated reactance winding in parallel rod configuration in PMSG design provides lower reactance and therefore, higher efficiency under wider load and frequency variation.

Key words: Special electrical machines, permanent magnet synchronous generator, compensate reactance, voltage, bifilar coil

INTRODUCTION

The topologies of classical generators are based on the electrical induction via the electric currents and magnetic fields inside a certain volume.[1,2] According to the literature, there are several different types of permanent magnet (PM) generators existing for different applications. However, the main classification is based on the machines' magnetic flux flow orientation between the magnet pole and core tip. The magnetic flux flow is either in radial or axial directions.[1,3] In comparison to axial flux machines, the radial flux ones have larger cogging torques, lower power densities and worse cooling systems.[1] Besides, the axial machines have simpler geometry and the possibility of multiple-rotor

(Received November 2, 2017; accepted February 17, 2018; published online February 28, 2018)

machine manufacturing on the same shaft. The iron core manufacturing is also easy for axial flux machines since the magnetic flux directly flows from one side of the machine to the other.[1,3]

From the operational point of view, an effective cooling system provides good efficiency for axial flux machines during long operational hours. While the radial flux generators require additional fan or blade structures, the axial flux machines have natural cooling systems due to the centrifugal transfer of the air mass from the central regions to the lateral regions.[4] The axial flux machines have larger windings' volumes then the radial flux ones in order to transfer heat to the lateral region.

One of the existent problems in terms of their manufacture is that the coil reactance X_L frequently becomes greater than the active resistance R_a of the armature coil. This design issue of generators creates obstacles to increased power output and efficiency of the generators. This problem could be solved by using a non-design method by using compensation of reactive power with capacitors.[5] However, this method requires additional installed equipment and its control while the load of the generator varies. The other opportunity to reduce the reactance of the generator at the stage of the design is to reduce the winding turns in the generator coils, but this method results in the reduction of the terminal voltage of the generator. The latter could be solved by increasing magnet volume or Hallbach array usage and, therefore, increasing the magnetic flux density.[6] All methods mentioned above have their positive and negative aspects. So in the study the alternative way of reducing the reactance of PMSG with the bifilar winding is presented.

The proposed PMSG should partially or negligibly reduce the reactance of the armature. It is claimed to have significant internal circuit reactance compensation by windings on the special coils by differing from earlier machines. Therefore, to perform the study of proposed topology PMSG, an electromagnetic design and analyses were performed by FEM.[7–15] The prototype machine has been designed with SolidWorks. EAGLE CAD has been used for the design of the electrical schematics. The experiments have been conducted in the laboratories of Klaipeda University.

The performed research and proposed design of PMSG with compensated reactance winding in parallel rod configuration will provide a possibility of lowering reactance and, therefore, to sustain higher efficiency under wider load and frequency variation. This also will provide showing the usage, farther study and optimization of such design PMSG.

DESIGN AND FINITE ELEMENT ANALYSIS OF THE PMSG

Initially, the present machine can have two types of configurations in terms of rods and coils as shown in Figs. 1 and 2. The configuration shown in Fig. 1a gives high voltages at the output with three phases. The second coil configuration (i.e., Fig. 1b) creates high currents, but lower voltages for the same rotation speed of PMSG.

The isometric view of the PMSG is shown in Fig. 2. The windings have two circular orientations side by side. The main interesting point is that the flux occurred by one winding affects the other windings. Half of this PMSG construction is unfolded into a linear type and modeled in a 2-D environment.

In order to calculate the fluxes and magnetic circuit parameters using FEM software, Fig. 3 has been sketched in FEMM software (a suite of programs for solving low frequency electromagnetic problems). The cores, relevant poles and windings of the PMSG section are shown in Fig. 3. The magnets from both sides are surface-mounted on the iron plate.

This proposed topology has four magnets for three stator rods or two pole pairs for three phases. The original orientation is to put ten PM on each of the four parts of the rotor. The aim is to lower the magnetic field interaction locally. If every second magnet from top and bottom of the PMSF rotor is eliminated, there is left only half of the area for the other magnet pole. The first one covers a full area causing high cogging torques in the operation. Thereby only, half of the flux from magnets is used. That issue has been solved by mounting 20 PM on each of the four parts of the rotor. With such a configuration of one coil wrapped with one pole (north for instance), the other two wraps 3 quarters

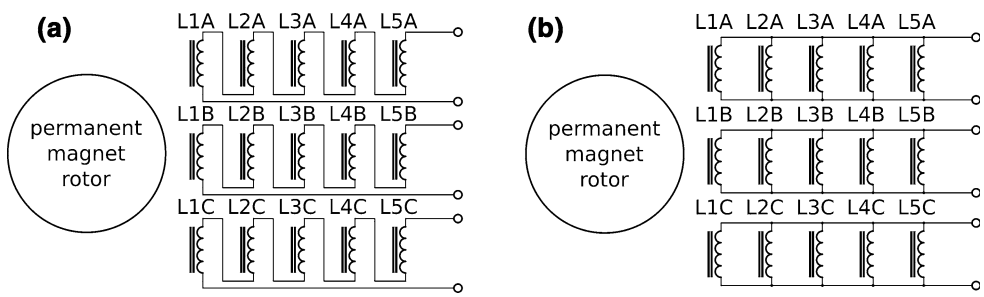

Fig. 1. (a) Serial and (b) parallel connection of the rods and windings.

of a south pole and a quarter of a north pole. This creates the magnetic force of the coil A equal to the magnetic forces of the coils B and C (Fig. 4; output from FEMM software).

A 3-D FEM analysis has been carried out in order to evaluate the magnetic field and to analyze the relation between the magnets and stator rods. In that manner, a 1/5 segment of the generator is shown below (Figs. 5a, b and 6a, b).

In general, the flux density maximizes around the magnets up to 1.2 T, whereas lower flux densities occur in the air gap and the inner volume of the cores. For the axial direction, the components and the flux densities are shown in Fig. 6a and b.

The flux densities of 1.2 T are found around the magnet and lowers to 0.4 T parts of magnetic core as in Fig. 6b. Several cross-section plots of the magnetic field are presented in Fig. 7a and b. According to radial and longitudinal sections in Fig. 7a, some PMSG parts of the components can have higher flux densities, which are not good for the field inhomogeneity. Some other regions can have moderate values such as 1.4 T. In Fig. 7b, the axial appearance fringes are shown. The field becomes 2 T just at the vicinity of PMs. However, the flux densities yield to 1.6 T in average for most of the rod surface.

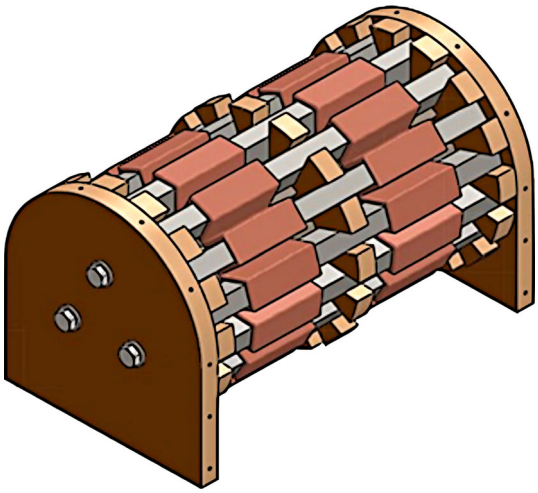

Fig. 2. 3-D isometric view of PMSG.

EXPERIMENTAL AND THEORETICAL DISCUSSION

The no-load results of the experiments provide the information of power losses in mechanical and magnetic (eddy currents) parts, the strength of the EMF induced. The curve in Fig. 8a is plotted to show the relationship of power loss and speed. All power losses consist of mechanical, magnetic and electric factors. The mechanical losses are caused by friction in bearings and ventilation. The magnetic losses occur due to core hysteresis and eddy currents. The electrical losses are occurring in the copper and depend on the square of the current. The no-load data plot of EMF versus speed curve is shown in Fig. 8b.

While the losses increase substantially via the rotation speed of the shaft or output frequency, the EMF linearly changes by the frequency. The plot is constructed from raw data to show the relationship of output characteristics $V_t = f(I_a,\ n)$ at different

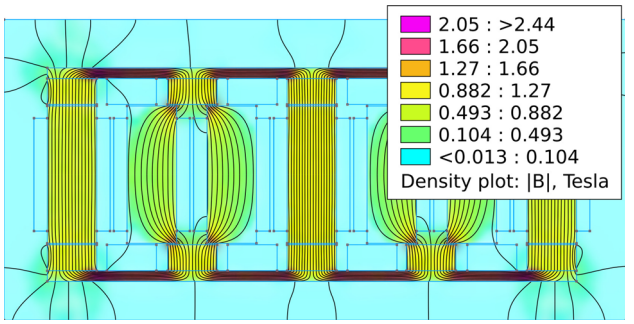

Fig. 4. Magnetic circuit flux lines of PMSG topology with double magnets.

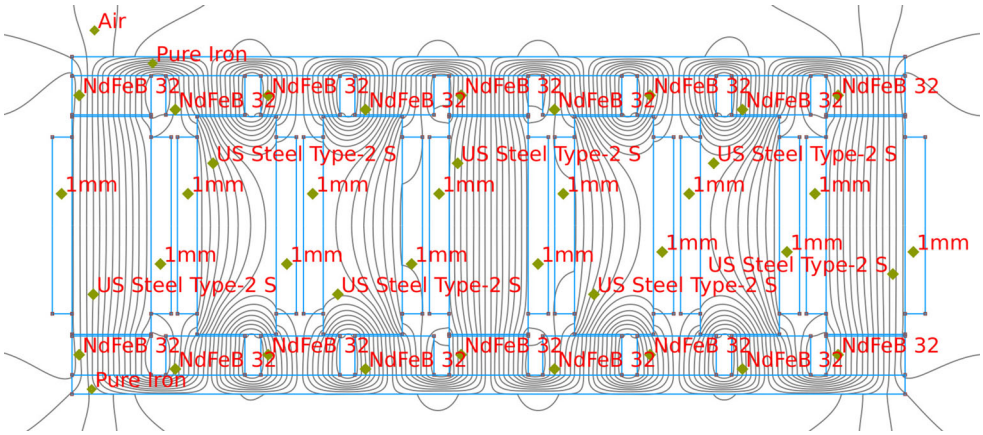

Fig. 3. Magnetic flux lines of the machine.

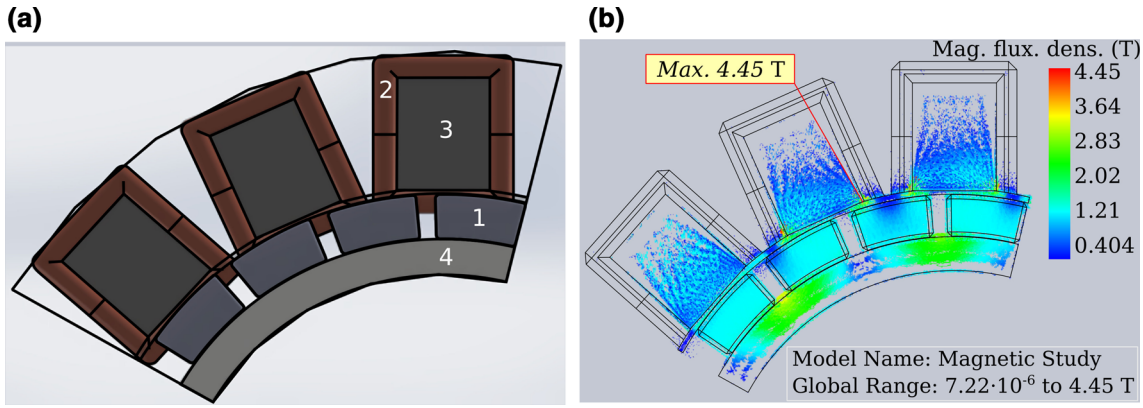

Fig. 5. (a) The 3-D sketch of windings and magnets of radial direction: 1-magnets, 2-windings, 3-ferromagnetic cores, 4-iron, or steel non-laminated core. (b) Flux density in PMSG.

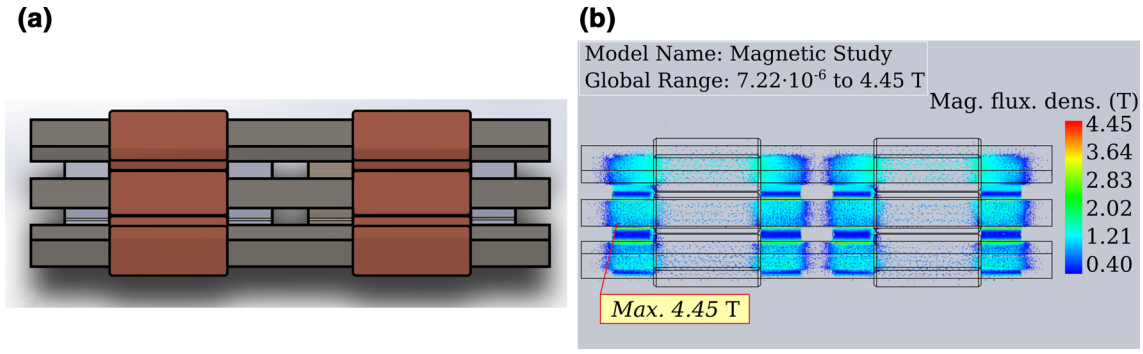

Fig. 6. (a) 1/5 segment of patented PMSG active material. (b) Magnetic flux density vector plot (top view).

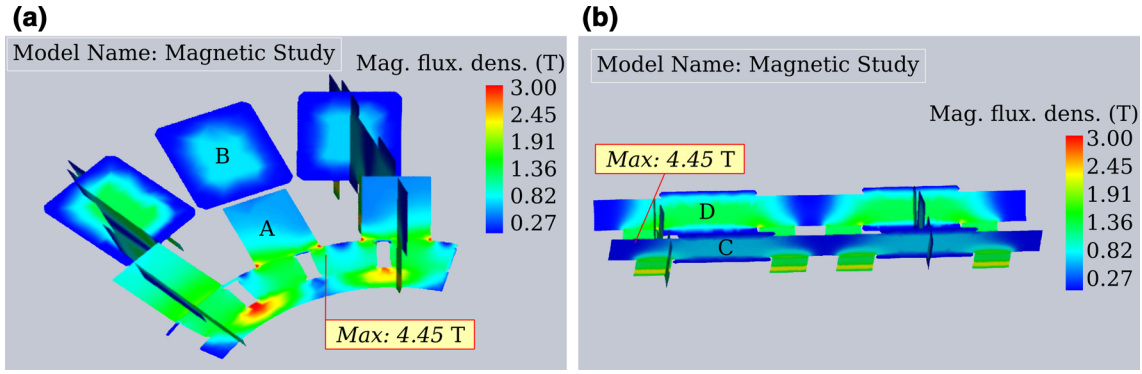

Fig. 7. Magnetic flux density continuous cross-section plots: (a) A: cross-section of magnet array; B: cross-section of coils. (b) C: axial section of core phase C; D: axial section of core phase A.

speeds. Armature active resistance is R_a = 0.317 Ω per phase.

The calculated parameters are presented in Table - I, where: f, E_f, X_s, I_{sc} and P_{out} denote frequency, EMF, short circuit current, synchronous reactance, and useful output power. The relation between the synchronous reactance X_s and frequency f is plotted in Fig. 9. A linear fitted line is also shown, and the equation describing the curve generated. This proves that there is no nonlinearity in PMSG stator circuit.

The achieved inductance is calculated as L = 17.1 ± 1.6 mH.

The terminal voltage of PMSG performance results are plotted in Fig. 10 and an interpolated surface plot is generated (Fig. 11). The voltages decrease via current to a certain value around 0 V and the current has the maximum value 12.5 A at a frequency of 114 Hz. When the frequency decreases, the voltage and current values also decrease with the similar trend.

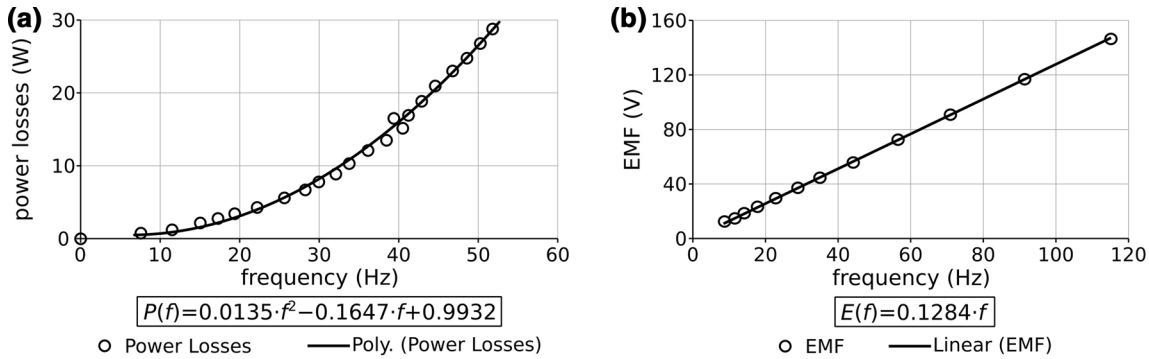

Fig. 8. (a) Mechanical and magnetic power losses and (b) EMF versus frequency.

Table I. The parameters of calculated curves

f, Hz	44.10	56.54	71.00	91.45	115.00
E_f, V	56.85	72.70	91.50	117.25	146.70
I_{sc}, A	10.95	12.13	12.06	12.03	12.58
X_s, Ω	5.18	5.99	7.58	9.74	11.66

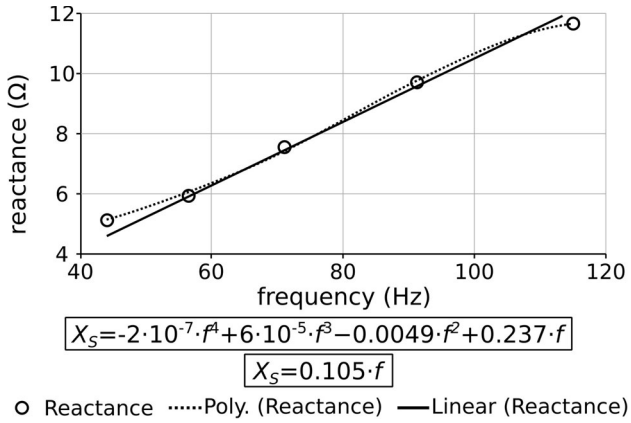

Fig. 9. Synchronous reactance versus frequency.

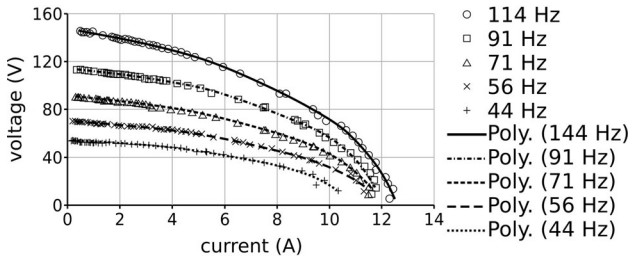

Fig. 10. Terminal output voltage versus load current at different frequencies.

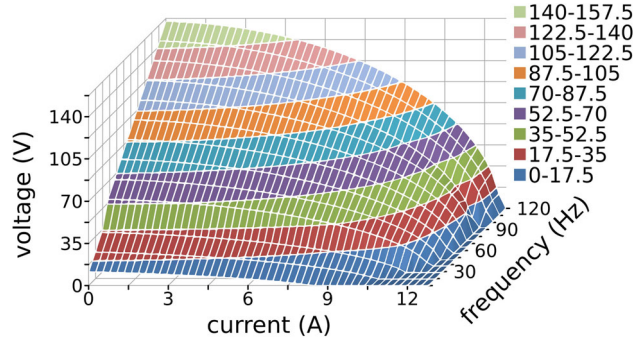

Fig. 11. Terminal output voltage versus load at different frequencies (surface plot).

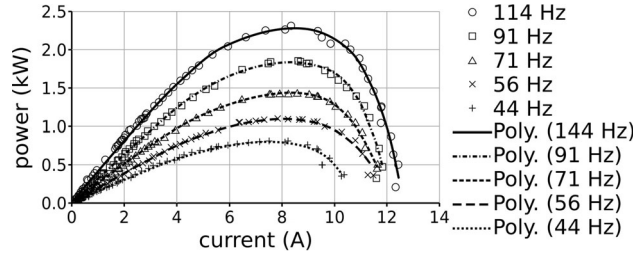

Fig. 12. Output power of PMSG versus load current at different frequencies.

In the 3-D appearance, that trend is more obvious. For "zero" current, the voltage increases linearly by frequency, whereas the increasing trend is lost for high currents (see in Fig. 11). The level line displays armature voltage drop by quarter ellipse trajectory because of synchronous reactance X_s of the system. The curve tends to straighten if more reactance is connected. Measured curves are lower than calculated due to asynchronous driving motor slip, during

the power load. The power output curves $P_{out} = f(I_a, f)$ have been calculated from $V_t = f(I_a, f)$ performance characteristics. Three-phase electric power of PMSG can be calculated by Eq. 1. This equation is used to calculate results (Fig. 12).

$$P_{out} = 3V_t I_a \cos\varphi \quad (1)$$

Evaluated measured maximum of output power is found as max P_{out} (8.33 A; 111.6 Hz) = 2334 W. The difference between a series connection of coils of PMSG maximum power output max P_{out} (1.6 A; 70.8 Hz) = 1414 W and in parallel max P_{out} (8.25 A; 70.65 Hz) = 1439 W were insignificant. This is due to the winding configuration. System has 15 rods and each of a phase has five independent rods with mutually winding coils. Thereby, it does not influence the output power by connecting them in parallel or series. Power output is shown on an interpolated surface plot in Fig. 13. When the frequency increases the output, power increases as well. For larger load currents, the maximum power is obtained.

The efficiency versus load current performance characteristics is shown in Fig. 14 for different speeds. The best performance point is obtained for the efficiency from 3 A to 10 A, which is very important for stable operation of the PMSG. In general, the rated current is around 7 A with 95% efficiency, which is a good result for proposed PMSG design. The frequency does not affect efficiency much at the rated current. But for low and high currents the frequencies have a different influence on efficiencies. The minimum frequencies have larger efficiencies for low current, whereas higher frequencies have high efficiency values with high current loads.

A 3-D surface plot (Fig. 15) is generated to have a better view in terms of efficiency, load current and frequency (i.e., speed). From the figure, it is clear that a better efficiency is obtained for high frequencies (i.e., speeds) with bigger currents.

In Table II, the parameters of the patented generator are shown. Table III gives the material features and obtained values. Thus, both the parallel and series connected information is obtained in the frame of that work.

Table IV gives the material properties for the construction.

CONCLUSIONS

The power no-load losses versus frequency characteristic is a square function of frequency that has been explored for a special PMSG. The analyzes include friction, ventilation and iron losses (induction, eddy currents). It has been proven that 100 W of power loss occurs at the speed 1380 rpm. The no-load EMF versus frequency characteristic has a linear relationship. Besides, when PMSG is loaded, terminal voltage falls by a quarter ellipse trajectory due to synchronous reactance X_s. Evaluated measured maximum of output power is found as max P_{out} (8.33 A; 111.6 Hz) = 2334 W. The difference between a series connection of coils of PMSG maximum power output max P_{out} (1.6 A; 70.8 Hz) = 1414 W and in parallel max P_{out} (8.25 A; 70.65 Hz) = 1439 W was insignificant. This is because the PMSG has 15 rods and each of phase has five independent rods with mutually winding coils. Thereby, it does not influence the output power by connecting them in parallel or series. The efficiency of the machine covers a large area at different frequencies (i.e., speeds) and load currents at $I_a = 7$ A provides the efficiency of $\eta \approx 95\%$. The greater the speed (i.e., frequency), the greater the load currents available for higher efficiencies. The nominal thermal current is limited up to practical

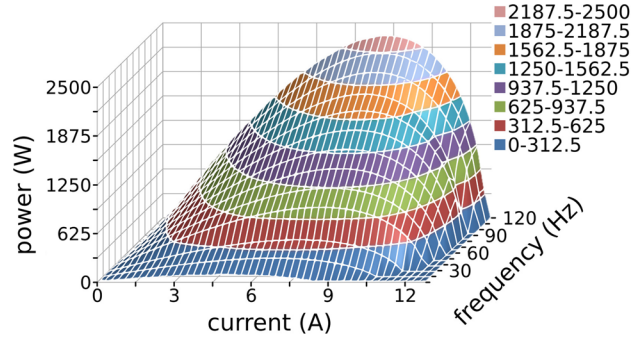

Fig. 13. Output power versus load at different frequencies (surface plot).

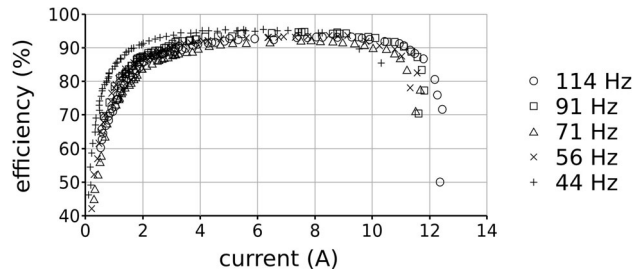

Fig. 14. PMSG efficiency versus load current at different frequencies.

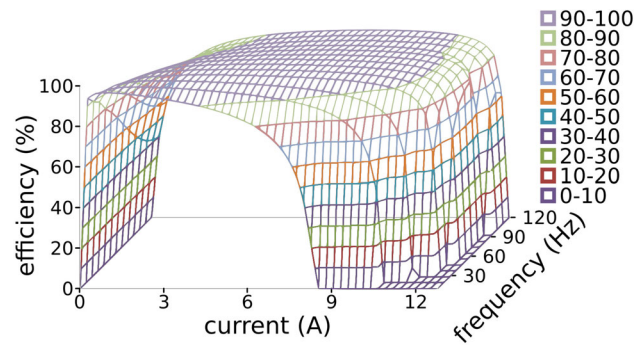

Fig. 15. Efficiency versus load current at different frequencies (surface plot).

Table II. Technical parameters and performance values of the PMSG topology with parallel rod configuration

Parameter	Value	Number of rotors	2
Load current	8.33 A	Number of poles (pair poles)	20 (10)
Output power	2334 W	Number of coils	30
Rated speed	1380 rpm	Number of loops per coil	375
No-load EMF	146.7 V	Active diameter	150 mm
Voltage at rated power	93.4 V	Rotor inertia	$29.58{\cdot}10^{-10}$ kg m^2
Efficiency	93.1%	Phase armature resistance	0.317 Ω
Rated power factor	0.66	Phase synchronous reactance	11.6 Ω
Total mass	55 kg	Phase inductance	(17.1 ± 1.6) mH
Output power per active mass	42.4 W/kg	Output frequency	70 Hz
Output power per volume	214.7 W/l	Cooling	Natural

Table III. Comparison with series parameters at 70 Hz

Parameter	Series value	Parallel value	Efficiency	92.4%	92.1%
Load current	1.65 A	8.25 A	Rated power factor	0.69	0.65
Output power	1414 W	1439 W	Phase armature resistance	8.7 Ω	0.317 Ω
No-load EMF	446 V	91.5 V	Phase synchronous reactance	186.7 Ω	11.6 Ω
Voltage at rated power	309 V	58.2	Phase inductance	442.5 mH	(17.1 ± 1.6) mH

Table IV. Consumed material quantities

Material	Mass (kg)	Number of pcs. or pkg.	NdFeB N45 magnets	3.3	80
Copper	13	30 coils	Getinax	10.3	5 parts
Laminated steel	20.7	15 rods 20 × 25 × 352	Polyethylene	1.8	2 cylindroids
Non-laminated steel	4.4	4 rings, 1 shaft, fasteners	Bearings	0.2	3

value I_{sc} = 12 A, $t^\circ \rightarrow 70°C$, This is needed because the magnet's Curie temperature is $t^\circ = 70°C$. The PMSG can be driven to produce S = 5.4 kVA in that respect. The research results shows that compensated reactance winding in parallel rod configuration in PMSG design provides lower reactance and therefore, higher efficiency under wider load and frequency variation.

ACKNOWLEDGEMENT

This paper was partially supported by the Agency of Science, Innovation and Technology of Lithuania using funding program "Inocekiai LT", Project No. VP2-1.3-UM-05-K. The authors acknowledge ElectroMagneticWorks Inc. for supporting trial license of ElectroMagneticWorks software (EMS), which is a SolidWorks add-on for electromagnetic analysis and simulation studies. The authors acknowledge the grant from The Ministry for European Affairs National Agency of Turkey under the Grant No: 2015-1-TR01- KA203-021342- Innovative European Studies on Renewable Energy Systems.

REFERENCES

1. H. Gör and E. Kurt, *Int. J. Hydrogen Energy* 41, 7005 (2016).
2. E. Kurt, H. Gör, and M. Demirtaş, *Energy Convers. Manag.* 77, 163 (2014).
3. E. Kurt, H. Gör, and U. Döner, *Int. J. Hydrogen Energy* 41, 7019 (2016).
4. C.H. Lim, G. Airoldi, R.G. Dominy, and K. Mahkamov, *Int. J. Therm. Sci.* 50, 2451 (2011).
5. S. Sayeef, N. Mendis, K. Muttaqi, and S. Perera, in *AUPEC Conference Proceedings* (2010), pp. 1–5.
6. H.A. Khazdozian, R.L. Hadimani, and D.C. Jiles, *Renew. Energy* 112, 84 (2017).
7. A.A. Pašilis and E. Guseinovienė, Bifilaric power generator or engine. LT Patent 5971 (2012).
8. J.E. Rucker, J.L. Kirtley, and T.J. McCoy, in *IEEE Electric Ship Technologies Symposium* (2005), pp. 451–458.
9. İ. Tarımer and C. Ocak, *Elektron. Elektrotech.* 92, 65 (2009).
10. Y. Chen, P. Pillay, and A. Khan, *IEEE Trans. Ind. Appl.* 41, 1619 (2005).
11. H. Vansompel, P. Sergeant, and L. Dupré, *IEEE Trans. Magn.* 46, 4101 (2010).
12. H. Kobayashi, Y. Doi, K. Miyata, and T. Minowa, in *Proceedings of Wind Energy Conference and Exhibition* (2009), pp. 4736–4744.
13. S. Hosseini, J.S. Moghani, N.F. Ershad, and B.B. Jensen, *IEEE T Magn.* 47, 772 (2011).
14. C.A. Oprea, C.S. Martis, F.N. Jurca, D. Fodorean, L. Szabo, and L. Szabó, in *ICCEP Conference Proceedings* (2011), pp. 588–592.
15. O.Lyan, E. Guseinoviene, A. Pasilis, A. Senulis, and A. Knolis, in *II European Workshop on Renewable Energy Systems Conference Proceedings* (2013), pp 1–6.